Controllable Synthesis of Conjugated Microporous Polymer Films for Ultra-sensitive Detection of Chemical Warfare Agents

Wanqi Mo
Northeast Forestry University
Yu Chen
Northeast Forestry University
Huaqian Liu
Northeast Forestry University
Zhiyong Cheng
Northeast Forestry University
Hongwei Ma (mahw@nefu.edu.cn)
Northeast Forestry University https://orcid.org/0000-0003-0128-0828
Xiaobai Li
Northeast Forestry University
Bin Li
Northeast Forestry University

Article

Keywords: chemical warfare, nerve agents, conjugated microporous polymer (CMP) films,

Posted Date: January 19th, 2021

DOI: https://doi.org/10.21203/rs.3.rs-141108/v1

Version of Record: A version of this preprint was published at Nature Communications on September 3rd, 2022. See the published version at https://doi.org/10.1038/s41467-022-32878-w.

Abstract

Nerve agents, one of the most toxic chemical warfare agents, seriously threaten human life and public security. The development of highly sensitive nerve-agent sensors has become an imperative and challenging topic. Reported here are two fluorescent conjugated microporous polymer (CMP) films, which show superior sensitivity for DCP (nerve-agent simulant). The limit of detection of TCzP-CMP can be determined as 13.2 ppt, which is the best report. This is due to the synergy of the susceptible "on-off" effect of hybridization and de-hybridization of hybrid local and charge transfer (HLCT) materials and the microporous structure of CMP films facilitating the inward diffusion of DCP vapor, and the “molecular wire effect”. This strategy provides a new idea for the future development of gas sensors. In addition, a portable sensor is successfully integrated based on TCzP-CMP films that enables wireless, remote, ultrasensitive, and real-time detection of DCP vapors.

Introduction

Organophosphorus nerve agents are an extremely toxic class of chemical warfare agents that can rapidly destroy the transmission of human nerve impulses due to their potent inhibition of the hydrolytic enzyme of neurotransmitter acetylcholine, causing paralysis of the central nervous system and eventually death[1, 2]. Despite the strict prohibition of nerve agents by the Chemical Weapons Convention, their recent use in the Syrian civil war and in the assassination of Sergei and his daughter Yulia shows a persistent threat to public security[3]. The development of efficient and reliable detection technologies for nerve agents, as one countermeasure of paramount importance, is therefore becoming an urgent topic, but also an arduous task because of their colorless, odorless, and volatile nature[4]. Furthermore, owing to the strong lethality, access to nerve agents is tightly restricted. Less poisonous simulants, e.g., diethyl chlorophosphate (DCP) is usually employed as substitutes of Sarin to facilitate the advance of detection technologies[5, 6]. Of various detection methods exploited, such as mass spectroscopy[7], ion mobility spectrometry[8], electrochemical sensors[9], and biosensors[10] fluorescent detection has galvanized interest due to numerous appealing virtues that include good portability, simple operation, high sensitivity, fast response, low cost, and real-time monitoring[11, 12].

Inspired by the mechanism that nerve agents inhibit the acetylcholinesterase (AChE) via reactions of their electrophilic phosphorus with the nucleophilic hydroxyl groups of AChE, fluorescent sensing materials with nucleophilic functional groups, including organic metal[13], *N*-based aromatic heterocycle[14], *N*- or *O*-containing compounds[15], have been studied during the last decade. Although fluorescent sensors are normally more sensitive than other detection strategies attributed to the fast photoinduced electron transfer (PET)[16] or fluorescence resonance energy transfer (FRET)[17] caused by phosphorylation resulting in fast changes of luminescence characteristic, even higher sensitivity is practically demanded because of the ultralow lethal dose (7 ppb) of Sarin. Recently, we first proposed a new type of nucleophilic fluorescent molecule with a hybrid local and charge transfer (HLCT) excited state, which has an impressive sensitivity for DCP vapors with a limit of detection (LOD) of 0.15 ppb, much lower than the

lethal dose, and a fast response of less than 1 s in saturated DCP vapors [18]. This is due to its peculiar hybrid state, which is highly susceptible to the attack of DCP, leading to a more rapid and effective fluorescent quenching response because of de-hybridization. Nevertheless, fluorescent small molecule materials for DCP frequently suffer from a common problem of serious photobleaching in sensor integration because of the unoptimistic anti-photobleaching ability, restricting their further applications[17].

In contrast, polymer fluorescent films possess preferable photostability. While, for solid-state sensing films, to realize efficient detection for trace amounts of nerve-agent vapors, the assistance of favorable gas capture capacity is desired. In a recent review, analyte diffusion into films is highlighted as a “critical” factor in the design of fast and responsive sensing systems[19]. Conjugated microporous polymers (CMPs) as a unique class of polymers featured by the extended π-conjugated system and inherent microporous structure have currently aroused increasing attention in a variety of research fields, for instance, organic optoelectronics[20], photocatalytic[21], gas adsorption and storage[22], as well as fluorescent sensing[23]. The micropores of CMPs are demonstrated to be beneficial to the inward diffusion of analytes, e.g., gas molecules and metal ions. Further, π-skeletons facilitate the exciton delocalization resulting in a “molecular wire effect” that is better able to amplify the fluorescence response signals and thus enhancing sensing sensitivity, compared with small molecular materials[24]. However, the film processability of CMPs limited by their poor solubility is the bottleneck issue in their practical applications[25]. Indeed, most studied fluorescence CMPs are insoluble solids that are unsuitable for sensor integration[26]. As is evident, challenges remain in developing a highly sensitive fluorescent material that has a desirable combination of good photostability, easy analyte diffusion and facile processability (i.e., ease of sensor implementation) for nerve-agent detection[27].

In our previous work, high-quality CMP fluorescence films were successfully fabricated by a simple electropolymerization (EP) method and the versatile sensing platforms were constructed[28, 29]. Building on this important result, herein, we propose a new strategy to access ultra-sensitive and photo-stable films for DCP vapors sensing (Fig. 1). Two HLCT molecules (TCz, TCzP) as the precursors with good electrochemical activity and different π-conjugated structure are designed and synthesized. The resulted TCz-CMP and TCzP-CMP films with different pore size, which directly affect the diffusion of DCP in the CMP films. What is exciting is that two CMP films are ultra-sensitive to DCP vapors, and the LOD of TCz-CMP and TCzP-CMP can be determined as 132 ppt and 13.2 ppt of DCP vapors, respectively, which are one to two orders of magnitude lower than that of the corresponding monomers. As far as we know, this is the best LOD of DCP vapors among fluorescent sensing materials reported so far. This excellent result is due to the efficient synergy of the excellent fluorescence response mechanism of HLCT, the "molecular wire effect" and the inward diffusion of DCP vapor. As a result, a portable sensor is successfully integrated based on TCzP-CMP films that enable wireless, remote, ultrasensitive, and real-time detection of DCP vapors. In particular, TCzP-CMP has a striking DCP adsorption capacity of up to 936 mg/g, which is ~3 times that of activated carbon, indicating a potential of combining nerve-agent detection with military protection.

Results

Optical properties of polymer precursors. In this contribution, two fluorescence materials TCz and TCzP composed of carbazole as donor and dibenzo [a, c] phenazine (DPPZ) as acceptor were designed (Supplementary Fig. 1). Compared with TCz, an additional phenyl ring is inserted between carbazole and DPPZ group for TCzP, the design strategy for extended π-conjugated structure is to increase locally emissive (LE) component in excited state and to optimize the size of the micropores in CMP obtained by EP. Then, the ultraviolet-visible (UV-Vis) absorption and photoluminescence (PL) properties of TCz and TCzP were investigated to understand the basic photophysical properties (Fig. 2a). TCzP and TCz show almost the same absorption peaks about 317 nm, which are ascribed to the π-π* of carbazole. As a comparison, the TCzP shows a narrower absorption band around 429 nm than that of TCz (445 nm), indicating to a more π-π* like character. For the PL spectra, TCz and TCzP give a yellow emission with λ_{max} at 553 nm and 548 nm, respectively, and the abnormal 5 nm blue-shift of TCzP compared to TCz in PL spectrum can be attributed to the enhanced LE component in the emissive state of TCzP[30].

To better understand the excited state properties, the solvatochromic effect of TCzP and TCz were further investigated. The PL spectra of TCzP and TCz show significant red-shift as the solvent polarity increases, which is the typical feature of the charge-transfer (CT) state. Moreover, the PL peaks of TCzP exhibit a larger red-shift (185 nm) than TCz (130 nm) from hexane (HEX), ethyl ether (ETE), dichloromethane (DCM) to acetonitrile (ACN), indicating that TCzP is more susceptible to external stimulation than TCz. Obviously, these features are expected to greatly help construct rapid and sensitive sensors (Fig. 2b). Generally, it is well-known that the photoluminescence quantum yield (PLQY) of CT molecules should be decreased with the increase in the solvent polarity because the high-polarity solvents could induce the stronger CT state and result in low PLQY. Unlike the common CT molecules, the two molecules show greatly enhanced PLQY with the increase of the solvent polarity, which is the result of the HLCT formation. Nevertheless, the CT-dominated HLCT state could occur in the large-polarity solvents, resulting in a decrease in PLQY (Supplementary Table. 1)[31].

In order to further clearly reveal the singlet state properties of TCz and TCzP, the linear relationships of the slope of Stokes shift ($v_a - v_f$) verse solvent polarity (f) using the Lippert-Mataga equation (Equation S3) were carried out (Fig. 2c) [32, 33]. In fact, two segmental fitting lines in TCz and TCzP represent the existence of two excited states. In low-polarity solvents (f<0.12), the lesser slope fitting lines with the small dipole moments (μ_e) are attributed to be LE state, while in high-polarity solvents (f>0.16), the higher slope fitting lines with large μ_e belong to CT state. As a comparison, TCzP has a larger μ_e (37.11 D) related to TCz (28.72 D), resulting that TCzP shows more obvious red-shift in the solvatochromic shift. In medium-polarity solvents, the energy levels of intrinsic LE and CT excited state are relatively close, and the coupling and crossing between the LE state and the CT state promote the formation of the HLCT state[34], which is consistent with solvatochromic results. In addition, the lifetime decay curves of TCz and TCzP in a medium-polarity solvent show a single exponential lifetime of 2.7 ns and 1.58 ns, respectively,

indicating that the HLCT excited state is a hybrid state, rather than a single mixed state of LE and CT (Fig. 2d).

Sensing performance and sensing mechanism of polymer precursors. The fluorescence response of the two small molecules with HLCT excited state to DCP vapors was investigated first. The fluorescence change of the TCzP and TCz spin-coated films in DCP vapors was monitored as a function of exposure time (Supplementary Fig. 6). It is worth noting that the two small molecule films are highly sensitive to DCP vapors due to the de-hybridization of HLCT excited state. The actual LOD of the two films can be evaluated as 1.32 ppb, which are one of the best reported so far (Supplementary Table. 3). To further examine and confirm the detection mechanism of TCz and TCzP to DCP vapors, the titration experiments of the ^{1}H NMR were performed. Upon addition of DCP to TCz and TCzP in $CDCl_3$, respectively, the chemical shifts of the protons on the DPPZ move to downfield, while no significant change for the other groups (Supplementary Fig. 7). This result may be attributed to the nucleophilic substitution reaction between TCz or TCzP and DCP, and the formed intermediate quickly undergoes a hydrolysis reaction with trace water, resulting in the protonation of the N atom in the DPPZ. Furthermore, ^{31}P NMR experiments were performed to reveal this hydrolysis process (Supplementary Fig. 8). Upon addition of TCz to DCP in $CDCl_3$, three new chemical shift peaks appear at 1.527 ppm, 0.630 ppm and -12.599 ppm, which correspond to the intermediate, diethyl phosphate and tetraethyl pyrophosphate (TEPP), respectively. According to previous reports[35], the TEPP is obtained through the nucleophilic substitution between diethyl phosphate and DCP, and diethyl phosphate is produced through the hydrolysis of intermediates with water. Therefore, the rational mechanism we speculated has been shown in Supplementary Fig. 9.

Calculated Excited State Properties. The quenching process of TCz and TCzP to DCP were confirmed by time-dependent density functional theory (TDDFT) calculations. Both the energy levels of the intermediate and protonation of two fluorescence molecules exhibits obviously decrease accompanied with satisfied quenching (Supplementary Fig. 10). The S_1 energy level difference of TCz (1.21 eV) before and after protonation is significantly smaller than that of TCzP (2.28 eV), indicating that TCzP is more sensitive to DCP than TCz. In addition, the energy level and the oscillator strength (f) of phosphorylated intermediates is lower than that of protonated products, which makes it possible to conclude that the two fluorescence molecules are more inclined to generate phosphorylated intermediates and then form protonated product. Then, the essence of their excited state quenching process was also revealed by natural transition orbit (NTO) in terms of S_1 excited states (Fig. 3). Before protonation, the S_1 transition of the two small fluorescence molecules is mainly the LE-dominated HLCT excited state, which is ascribed to S_1 transition of DPPZ. After protonation, the vertical electron effect of the TCz and TCzP is forbidden, resulting in the intra-molecular charge transfer (ICT) transitions, which correspond to the new absorption peak at 592 nm and 521 nm in the absorption spectrum, respectively (Supplementary Fig. 11). In this case, the uniform HLCT state of the two fluorescence molecules becomes a separate LE state and CT state, leading to a significant fluorescence quenching. Upon addition of DCP into the two fluorescence molecules, their fluorescence lifetime recorded by transient PL spectra enhances significantly, indicating the S_1 transition is forbidden while generating a new none-emissive CT state (Supplementary Fig. 12),

which is agreement with the results by the NTO calculation. However, the two fluorescence films faced serious photo-bleaching problems, which greatly shorten the working life of these films and are not suitable for device integration.

The preparation of CMP films and pore size analysis. In order to further improve the detection performance and the optical stability of these films, the CMP films were prepared by cyclic voltammetry (CV) in a standard three-electrode electrochemical cell[36]. In the single-cycle CV curve, the initial oxidation potentials of TCz and TCzP are observed at 1.03 V and 0.98 V, which are attributed to the oxidation of carbazole group. As the scanning potential increases to 1.11 V and 1.03 V in TCz and TCzP, respectively, indicating more carbazole groups were oxidized and produce more carbazole radical cations (Fig. 4a). Then, an oxidation potential appears at 1.12 V for TCzP, which is assigned to the oxidation of the benzene ring connected to carbazole. As the scanning potential continues to increase, TCz and TCzP generate a peak potential at 1.23 V and 1.35 V, respectively, indicating that DPPZ was oxidized. During the negative scan, two obvious reduction peaks of TCz are observed at 0.88 V and 1.09 V, which correspond to the reduction of dimeric carbazole cations and DPPZ. Correspondingly, the reduction peaks of TCzP are located at 0.74 V and 1.01 V. Accordingly, the high oxidation potentials of 1.2 V and 1.1 V were selected for the preparation of TCz-CMP and TCzP-CMP films, respectively (Supplementary Fig. 13). This oxidation potential can ensure the effective coupling reaction of the carbazole groups while avoiding the oxidation of DPPZ to increase the fluorescence intensity of the CMP films. In this case, the oxidation of carbazoles forms carbazole cation radicals which can quickly undergo a coupling reaction with a neutral carbazole to form a dimeric carbazole cation with a lower oxidation potential, and CMP films are obtained by the redox reaction of the dimeric carbazole cations. In the multicycle CV curves of TCz and TCzP, the increase of the reduction peak indicates that the CMP films are starting to be deposited on the electrode, which is the proof of the formation of CMP films (Supplementary Fig. 13). The CMP films with uniform surface morphology can be observed by high-resolution transmission electron microscope (HRTEM) (Supplementary Fig. 14). Moreover, the film thickness of TCz-CMP and TCzP-CMP can be precisely controlled by scanning cycles. It can be seen that for TCz-CMP and TCzP-CMP films, the film thickness has a good linear relationship with the scanning cycles and increases by 1.05 nm and 2.95 nm per scanning cycle, respectively (Supplementary Fig. 15). The formation of TCz-CMP and TCzP-CMP films were further confirmed by Fourier transform infrared (FT-IR) spectroscopy (Supplementary Fig. 16). TCz-CMP and TCzP-CMP show a new peak appears about 804 nm that is assigned to dimeric carbazole, whereas the absorption peaks of DPPZ at 766 nm and 775 nm were almost unchanged before and after EP, indicating that the oxidation of carbazole did not affect DPPZ. In addition, the powder X-ray diffraction (XRD) patterns of TCz-CMP and TCzP-CMP demonstrate a broad and dispersion peak within the 2θ range of 5-40° (Supplementary Fig. 17), indicating the amorphous feature of CMP films, which is expected for the preparation of the CMP films.

To further study the microporous structure of TCz-CMP and TCzP-CMP, we conducted nitrogen adsorption/desorption experiments and evaluated their porosity at 77.3 K (Fig. 3b). Both TCz-CMP and TCzP-CMP show typical i-type and iv-type nitrogen adsorption isotherms according to the IUPAC

classification. The obtained curve shows that nitrogen uptake increases sharply at low relative pressure (p/p_0 less than 0.05), which indicates the existence of a microporous structure. Under relative high pressure (0.4-1.0), the hysteresis loop shows the coexistence of micropores and mesopores. The Brunauer-Emmett-Teller (BET) surface area and a total pore volume were calculated to be 407 m^2/g and 1.29 cm^3/g for TCzP-CMP. In a comparison, TCz-CMP has a smaller BET surface area (137 m^2 /g) and total pore volume (0.12 cm^3/g). Correspondingly, the pore size distributions of TCzP-CMP and TCz-CMP are 0.81-1.0 nm and 0.71-0.74 nm, respectively (Fig 4c). After the optimization by TDDFT, the possible microporous structures of TCzP-CMP and TCz-CMP were obtained (Fig. 4d). However, the pore size of TCz-CMP is smaller than that of DCP (0.84 nm), which is not conducive to the diffusion of DCP into the interior. In contrast, the pore size of TCzP-CMP is suitable for the diffusion of DCP.

Adsorption performance test of CMP. The adsorption capacity of CMP to the analytes is an important factor affecting the sensing performance, so a simple self-made adsorption system was first built to evaluate the adsorption capacity of TCz-CMP and TCzP-CMP to DCP vapors (Supplementary Fig. 18). It is found that the adsorption capacity of the two CMP to DCP vapors increases rapidly within 200 min, which is attributed to the existence of sufficient action sites in CMP (Fig. 5a). Then, as the exposure time prolonged, the adsorption capacity shows a slow tendency, which is attributed to that most sites are occupied, resulting that the adsorption rate gradually decreases and finally reaches equilibrium at 1400 min. The maximum adsorption capacity of TCzP-CMP can reach 936 mg/g, while TCz-CMP is only 75 mg/g. This may be because TCzP-CMP has a larger pore structure and specific surface area than TCz-CMP, which is more conducive to the diffusion of DCP molecules into CMP. Then, in order to understand the adsorption process in depth, the adsorption kinetics were evaluated using the pseudo first-order (PFO) (Equation 1), pseudo-secondary (PSO) (Equation 2) model and intra-particle diffusion model (Equation 3)[37, 38].

Comparing the two correlation coefficients (R^2) of TCz-CMP and TCzP-CMP to DCP vapors, the PSO model (R^2>0.99) has better correlation than the PFO model (R^2 <0.96), which indicates that the PSO model is more suitable for describing the adsorption process for DCP than the PFO model (Fig. 5b-c). The results show that the adsorption of DCP by TCz-CMP and TCzP-CMP is a chemical adsorption process, which may depend on the nucleophilic substitution reaction and electronic interaction between the two CMPs and DCP[37]. The experimental adsorption capacity of TCz-CMP of 78 mg/g is much lower than that of TCzP-CMP (936 mg/g), once again proving that the pore size directly affects the diffusion of DCP. The calculated equilibrium adsorption capacity q_e (976 mg/g) of TCzP-CMP is close to the experimental value. Furthermore, the intraparticle diffusion model is adopted to fit experimental data, revealing the rate-controlling steps in the DCP adsorption process. It can be observed that there are two linear relationships in the entire time range of the adsorption process, which indicate that surface adsorption and intraparticle diffusion synergistically affect the adsorption process (Fig. 5d). For TCzP-CMP, the fitting line of intra-particle diffusion almost passes through the origin (C_1=6), which proves that the intra-particle diffusion of TCzP-CMP is a speed-controlled step in the first adsorption stage of DCP, and there may be no boundary effect. Concurrently, we were surprised to find that TCzP-CMP not only has good adsorption

performance for DCP vapors, but also for other CWA simulants, such as DCNP, DMMP, TEP and 2-CEES. Similarly, the adsorption kinetics of PFO, PSO and intraparticle diffusion models were evaluated (Supplementary Fig. 19). It can be seen that the adsorption of these CWA analogs by TCzP-CMP is more consistent with the PSO model, which may depend on the point-to-dipole π interaction[37, 39] (Supplementary Table. 4-5). More importantly, it has been proved that the adsorption capacity of these five CAW simulants by TCzP-CMP is 2-3 times that of activated carbon (Supplementary Table. 6). Therefore, this TCzP-CMP as the adsorption material for CWA has potential application in military protection.

Optical properties of CMP films. Compared with the spin-coated films of TCz and TCzP monomers, the emission peaks of TCz-CMP and TCzP-CMP films are red-shifted by 60 nm and 41 nm, respectively, which are ascribed to the extended π-conjugate structure (Supplementary Fig. 20). To study the fluorescence stability of these two CMP films, the TCz-CMP films and TCzP-CMP films were continuously irradiated under the excitation light with the maximum excitation wavelength at 450 nm and 440 nm for 90 s. The fluorescence intensity of the TCz-CMP films nearly has no changes, while that of the TCzP-CMP films is only quenched by 7%. Both the TCz-CMP and TCzP-CMP films demonstrate much better stability than their monomers films because of their cross-linked structure, thus effectively overcoming the photobleaching problems, which is fully satisfactory for practical applications (Supplementary Fig. 21).

Sensing performance of CMP films. The fluorescence response of these two CMP films to DCP vapors was investigated (Fig. 6a-b). The actual LOD of TCz-CMP can be determined to be 132 ppt, which is an order of magnitude lower than monomer spin-coated films. The excellent can be attributed to the susceptible "on-off" effect of hybridization and dehybridization of HLCT materials, and the "molecular wire effect". As a comparison, the LOD of TCzP-CMP (13.2 ppt) is an order of magnitude lower than that of TCz-CMP. This enhanced detection performance can be ascribed the diffusion of DCP into the CMP films. The coefficient of determination (R^2) of TCz-CMP (0.9996) and TCzP-CMP (0.9850) films shows that the stability of these films can effectively improve the detection accuracy (Fig. 6c-d). Importantly, TCz-CMP and TCzP-CMP films have a rapid response to the low concentration of DCP vapors within 2.1 s and 5 s (Fig. 6e-f), which fully meets the requirements of real-time detection. Furthermore, it is found that the two quenched CMP films by high-concentration of DCP vapors (1.32 ppm) were degassed in a vacuum oven at 50 ℃ for 2 h, the fluorescence intensity of the two CMP films can be restored to the original level, respectively. Even though recycled six times, the two CMP films still show a good response to DCP vapors (Fig. 6g-h). In a comparison, TCzP-CMP films exhibit better self-recovery than TCz-CMP films, which may be due to the fact that the pore size of the TCzP-CMP films is larger than that of the TCz-CMP films and DCP molecules, which facilitate the escape of DCP molecules under vacuum conditions. Further the fluorescence response of the two CMP films to the possible interferences was investigated. Upon exposure to DCP (1.32 ppm), ethanol (780 ppm), water (32000 ppm), trifluoroacetic acid (TFA 13 ppm), DCNP (2 ppm), DMMP (200 ppm), triethylamine (1090 ppm), 2-CEES (38 ppm), pyridine (25 ppm), acetone (816 ppm), n-hexane (21 ppm) vapors and toluene (140 ppm), respectively, the

TCz-CMP and TCzP-CMP films exhibit higher selectivity to DCP vapors than other interferences (Supplementary Fig. 22).

System assembly and testing. To verify the practical applicability of CMP films, a portable fluorescent detection systems consisted of intake pump, TCzP-CMP films, LED (365 nm), optical recognition detection system, Bluetooth transceiver, and an optimized sealed cavity was built (Fig. 7a, c). The working principle of the device is as follows: using STM32 as the Microcontroller Unit (MCU), controlling the switch of the air pump and driving the linear array CCD sensor to collect signals, and then send the signals to the upper computer (PC) through the Bluetooth transceiver (Fig. 7b). The switch of the LED light is synchronized with the CCD signal collection. Then, the various level of DCP vapors were injected into the sealed cavity for 10 seconds through the intake pump and the fluorescence signal was analyzed by operating software. It can be observed that the changes of fluorescence intensity to DCP vapors show a good linearity (R^2=0.98), and the LOD can be determined as 13.2 ppt (Fig. 7d). In addition, the portable fluorescence detection systems with a Bluetooth device can realize remote and wireless monitoring the DCP vapors, thereby avoiding the risk of direct detection by personnel. The fluorescent system equipped with TCzP-CMP films show rapid and sensitive performances for DCP detection, indicating that they can fully meet the requirements of practical applications.

Discussion

In conclusions, two fluorescent molecules (TCz and TCzP) with HLCT excited state were successfully synthesized, and show high sensitivity to DCP vapors. Both the LOD of TCz and TCzP can be determined to 1.32 ppb, which are one of the best reported so far. In order to overcome the photobleaching problem of these two molecules and explore the influence of microstructure on sensing, two CMP films (TCz-CMP, TCzP-CMP) were prepared using TCz and TCzP as precursor molecules through a simple and effective EP method. In the absence of microporous diffusion, based on the synergistic effect of the susceptible "on-off" effect of HLCT material and the "molecular wire effect", the TCz-CMP films are hypersensitive to DCP vapors. The LOD can be determined to be 132 ppt, which is 1/10 of its spin-coated films. Conversely, there are microstructures in TCz-CMP films that is suitable for the diffusion of DCP, their LOD is once again reduced by one order of magnitude (13.2 ppt) than that of TCz-CMP films. This strategy provides a new idea for the future development of gas sensors. Accordingly, the TCzP-CMP films are implanted in a self-built portable detection system, which realizes remote and wireless detection of DCP with the LOD of 13.2 ppt and verifies the practical application of the TCzP-CMP films. In addition, the equilibrium adsorption capacity of TCzP-CMP can reach to 936 mg/g, which is ~3 times that of activated carbon. Therefore, TCzP-CMP has the promising dual-functional materials of DCP sensing and military protection.

Methods

Synthesis of compounds TCz. A mixture of 3,6,11-tribromodibenzo[a,c]phenazine 517 mg (1 mmol), carbazole 1004 mg (3 mmol), CuI 38 mg (0.2 mmol), trans-1,2-Diaminocyclohexane 980 μL (8 mmol), K_3PO_4 955 mg (4.5 mmol), and dry toluene 100 mL was added into a 250 mL flask. Vacuum to remove

air under liquid nitrogen freezing, and then reflux for 48 h under nitrogen protection. After cooling to room temperature, it was extracted with dichloromethane/water, and the organic layer was dried with $MgSO_4$. The mixture was purified through a silica gel column, using dichloromethane/petroleum ether (v/v=1:4) as the eluent, the crude product obtained was recrystallized with toluene/anhydrous methanol, and orange-yellow powder (316 mg) was obtained with a yield of 41%. ^{1}H NMR (500 MHz, $CDCl_3$) 9.75 (2 H, dd, J 18.7, 8.6), 8.74 (2 H, s), 8.68 – 8.60 (2 H, m), 8.29 – 8.13 (7 H, m), 8.07 (2 H, dd, J 13.8, 8.5), 7.74 (2 H, d, J 8.0), 7.61 (4 H, t, J 7.2), 7.52 (2 H, t, J 7.7), 7.43 (6 H, dt, J 15.7, 7.3), 7.33 (4 H, dd, J 12.8, 7.0).

The synthesis of compound TCzP. K_2CO_3 2488 mg (162 mmol), water 54 mL, ethanol 35 mL and toluene 100 mL were added to a 500 mL flask. Next, the mixture of 3,6,11-tribromodibenzo[a,c]phenazine 517 mg (1 mmol), (4-(9H-carbazol-9-yl)phenyl) boronic acid 1291 mg (4.5 mmol)), Pd $(PPh_3)_4$ 173 mg (0.15 mmol) was added, and applying vacuum to remove air under the liquid nitrogen freezing, and then react at 85 °C for 48 hours under nitrogen protection. After cooling to room temperature, it was extracted with Toluene/water, and the organic layer was dried with $MgSO_4$. The mixture was purified by silica gel column using dichloromethane/petroleum ether (v/v=1:1.5) as the eluent to obtain the crude product. Toluene/anhydrous methanol was recrystallized to obtain yellow powder with a yield of 53% (532 mg). ^{1}H NMR (500 MHz, $CDCl_3$) 9.66 – 9.55 (2 H, m), 8.98 (2 H, s), 8.70 (1 H, d, J 1.9), 8.50 (1 H, d, J 8.7), 8.27 (1 H, dd, J 8.8, 2.0), 8.19 (6 H, t, J 6.9), 8.16 – 8.13 (2 H, m), 8.13 – 8.08 (6 H, m), 7.83 – 7.76 (6 H, m), 7.59 – 7.52 (6 H, m), 7.50 – 7.44 (6 H, m), 7.34 (6 H, dd, J 15.4, 8.1).

Preparation of CMP films. CMP films was prepared using a CH Instruments CHI660E electrochemical analyzer in three-electrode system. The reference electrode, working electrode and counter electrode correspond to Ag/Ag^+ non-aqueous electrode, indium tin oxide (ITO) and titanium plate. The electrolyte solution is a mixture of precursor molecule (TCz or TCzP) and tetrabutylammonium hexafluorophosphate (0.1 M), and the dry dichloromethane is used as the solvent. Here, the concentrations of TCz and TCzP are 5×10^{-5} M and 4×10^{-4} M, respectively, and the multi-cycle cyclic voltammetry was adopted for the preparation.

The bulky samples were obtained by chemical oxidation with ferrous (III) chloride[28]. The fluorescent material (TCz or TCzP) monomer was dissolved in the chloroform solution, and then added dropwise to the chloroform suspension containing ferric chloride. After stirring for 48 hours, the insoluble solid was filtered and purified by methanol using a Soxhlet extractor for 24 hours. The resulting powder yields were 53% (TCz-CMP) and 79% (TCzP-CMP).

Adsorption kinetics formula. The pseudo first-order (PFO) (Equation 1), pseudo-secondary (PSO) (Equation 2) model and intra-particle diffusion model (Equation 3) is as follows[37]:

$$\ln(q_e - q_t) = \ln q_e - k_1 t \quad (1)$$

$$\frac{1}{q_t} = \frac{1}{k_2 q_e^2} + \frac{t}{q_e} \quad (2)$$

$$q_t = k_i t^{1/2} + C \quad (3)$$

where t is the exposure time (h), q_t (mg/g) and q_e (mg/g) represent the adsorption capacity of DCP at time t and equilibrium, respectively. k_1 (1/h), k_2 (g/(mg h)), k_i (mg/(g $h^{1/2}$)) refer to the rate constant, and C (mg/g) is the intercept, which reflects the boundary layer effect.

Declarations

Data availability

The data that support the findings of this study are available from the corresponding author upon reasonable request.

Acknowledgements

We are grateful for the financial supported by the National Science Foundation of China (51903031), Natural Science Foundation of Heilongjiang Province (YQ2019E003), China Postdoctoral Science Foundation Funded Project (2018M630331; 2019T120249), the 111 Project (B20088).

Author contributions

H. Ma, B. Li and X. Li. conceived the concepts for the research project. W. Mo performed material synthesis, fluorescence testing, equipment fabrication and data analysis. Y. Chen performed a gas adsorption test. H. Liu and Z. Cheng performed theoretical calculations. H. Ma, X. Li and W. Mo wrote the manuscript. All authors discussed the results and commented on the manuscript.

Competing interests

The authors declare no competing interests

Additional information

Supplementary information is available for this paper at

References

1. Mercey G*, et al.* Reactivators of Acetylcholinesterase Inhibited by Organophosphorus Nerve Agents. *Acc. Chem. Res.* **45**, 756-766 (2012).
2. Stone R. How to defeat a nerve agent. *Science* **359**, 23-23 (2018).

3. K. SL. Nerve agents: from discovery to deterrence. *Nature* **583**, 28-29 (2020).\
4. Sambrook MR, Notman S. Supramolecular chemistry and chemical warfare agents: from fundamentals of recognition to catalysis and sensing. *Chem. Soc. Rev.* **42**, 9251-9267 (2013).
5. Zhou X, Zeng Y, Liyan C, Wu X, Yoon J. A Fluorescent Sensor for Dual-Channel Discrimination between Phosgene and a Nerve-Gas Mimic. *Angew.Chem. Int. Ed.* **55**, 4729-4733 (2016).
6. Bencic-Nagale S, Sternfeld T, Walt DR. Microbead Chemical Switches: An Approach to Detection of Reactive Organophosphate Chemical Warfare Agent Vapors. *J. Am. Ceram. Soc.* **128**, 5041-5048 (2006).
7. Steiner WE, Klopsch SJ, English WA, Clowers BH, Hill HH. Detection of a Chemical Warfare Agent Simulant in Various Aerosol Matrixes by Ion Mobility Time-of-Flight Mass Spectrometry. *Anal. Chem.* **77**, 4792-4799 (2005).
8. Maziejuk M, Ceremuga M, Szyposzyńska M, Sikora T, Zalewska A. Identification of organophosphate nerve agents by the DMS detector. *Sens. Actuators, B* **213**, 368-374 (2015).
9. Taranekar P, Baba A, Park JY, Fulghum TM, Advincula R. Dendrimer Precursors for Nanomolar and Picomolar Real-Time Surface Plasmon Resonance/Potentiometric Chemical Nerve Agent Sensing Using Electrochemically Crosslinked Ultrathin Films. *Adv. Funct. Mater.* **16**, 2000-2007 (2006).
10. Goud KY*, et al.* OPAA/fluoride biosensor chip towards field detection of G-type nerve agents. *Sens. Actuators, B* **320**, 128344 (2020)
11. Chen L, Liu D, Peng J, Du Q, He H. Ratiometric fluorescence sensing of metal-organic frameworks: Tactics and perspectives. *Coord. Chem. Rev.* **404**, 213113 (2020).
12. Julià López A, Ruiz-Molina D, Landfester K, Bannwarth MB, Roscini C. Off/On Fluorescent Nanoparticles for Tunable High-Temperature Threshold Sensing. *Adv. Funct. Mater.* **28**, 1801492 (2018).
13. Cao M*, et al.* Porphyrinic Silver Cluster Assembled Material for Simultaneous Capture and Photocatalysis of Mustard-Gas Simulant. *J. Am. Ceram. Soc.* **141**, 14505-14509 (2019).
14. Yao J*, et al.* Concise and Efficient Fluorescent Probe via an Intromolecular Charge Transfer for the Chemical Warfare Agent Mimic Diethylchlorophosphate Vapor Detection. *Anal. Chem.* **88**, 2497-2501 (2016).
15. Lei Z, Yang Y. A Concise Colorimetric and Fluorimetric Probe for Sarin Related Threats Designed via the “Covalent-Assembly” Approach. *J. Am. Ceram. Soc.* **136**, 6594-6597 (2014).
16. Dale TJ, Rebek J. Fluorescent Sensors for Organophosphorus Nerve Agent Mimics. *J. Am. Ceram. Soc.* **128**, 4500-4501 (2006).
17. Xiong W, Gong Y, Che Y, Zhao J. Sensitive Discrimination of Nerve Agent and Sulfur Mustard Simulants Using Fluorescent Coassembled Nanofibers with Förster Resonance Energy Transfer-Enhanced Photostability and Emission. *Anal. Chem.* **91**, 1711-1714 (2019).
18. Li X*, et al.* Visualization of Ultrasensitive and Recyclable Dual-Channel Fluorescence Sensors for Chemical Warfare Agents Based on the State Dehybridization of Hybrid Locally Excited and Charge

Transfer Materials. *Anal. Chem.* **91**, 10927-10931 (2019).

19. Fan S*, et al.* Challenges in Fluorescence Detection of Chemical Warfare Agent Vapors Using Solid-State Films. *Adv. Mater.* **32**, 1905785 (2020).
20. Gu C*, et al.* Electrochemical Route to Fabricate Film-Like Conjugated Microporous Polymers and Application for Organic Electronics. *Adv. Mater.* **25**, 3443-3448 (2013).
21. Wang L*, et al.* Conjugated Microporous Polymer Nanosheets for Overall Water Splitting Using Visible Light. *Adv. Mater.* **29**, 1702428 (2017).
22. Du R, Zheng Z, Mao N, Zhang N, Hu W, Zhang J. Fluorosurfactants-Directed Preparation of Homogeneous and Hierarchical-Porosity CMP Aerogels for Gas Sorption and Oil Cleanup. *Adv. Sci.* **2**, 1400006 (2015).
23. Liu X, Xu Y, Jiang D. Conjugated Microporous Polymers as Molecular Sensing Devices: Microporous Architecture Enables Rapid Response and Enhances Sensitivity in Fluorescence-On and Fluorescence-Off Sensing. *J. Am. Ceram. Soc.* **134**, 8738-8741 (2012).
24. Fan L-J*, et al.* Fluorescent conjugated polymer molecular wire chemosensors for transition metal ion recognition and signaling. *Coord. Chem. Rev.* **253**, 410-422 (2009).
25. Zhou Z*, et al.* Electropolymerization of robust conjugated microporous polymer membranes for rapid solvent transport and narrow molecular sieving. *Nat. Commun.* **11**, 5323 (2020).
26. Gu C, Huang N, Gao J, Xu F, Xu Y, Jiang D. Controlled Synthesis of Conjugated Microporous Polymer Films: Versatile Platforms for Highly Sensitive and Label- Free Chemo- and Biosensing. *Angew.Chem. Int. Ed.* **53**, 4850-4855 (2014).\
27. Fan S*, et al.* Challenges in Fluorescence Detection of Chemical Warfare Agent Vapors Using Solid-State Films. *Adv. Mater.* **32**, 1905785 (2020).
28. Liu H*, et al.* Dendrimer-Based, High-Luminescence Conjugated Microporous Polymer Films for Highly Sensitive and Selective Volatile Organic Compound Sensor Arrays. *Adv. Funct. Mater.* **30**, 1910275 (2020).
29. Ma H*, et al.* A Dendrimer-Based Electropolymerized Microporous Film: Multifunctional, Reversible, and Highly Sensitive Fluorescent Probe. *Adv. Funct. Mater.* **26**, 2025-2031 (2016).
30. Zhang S*, et al.* Achieving a Significantly Increased Efficiency in Nondoped Pure Blue Fluorescent OLED: A Quasi-Equivalent Hybridized Excited State. *Adv. Funct. Mater.* **25**, 1755-1762 (2015).
31. Zhou C*, et al.* Enhancing the Electroluminescent Efficiency of Acridine-Based Donor–Acceptor Materials: Quasi-Equivalent Hybridized Local and Charge-Transfer State. *J. Phys. Chem. C* **122**, 18376-18382 (2018).
32. Noboru M, Yozo K, Masao K. Solvent Effects upon Fluorescence Spectra and the Dipolemoments of Excited Molecules. *Bull. Chem. Soc. Jpn.* **29**, 465-470 (1956).
33. Lippert E. Spektroskopische Bestimmung des Dipolmomentes aromatischer Verbindungen im ersten angeregten Singulettzustand. *Zeitschrift für Elektrochemie, Berichte der Bunsengesellschaft für physikalische Chemie* **61**, 962-975 (1957).

34. Li W, *et al.* Employing ~100% Excitons in OLEDs by Utilizing a Fluorescent Molecule with Hybridized Local and Charge-Transfer Excited State. *Adv. Funct. Mater.* **24**, 1609-1614 (2014).
35. Jang YJ, Tsay OG, Murale DP, Jeong JA, Segev A, Churchill DG. Novel and selective detection of Tabun mimics. *Chem. Commun.* **50**, 7531-7534 (2014).
36. Li X, Li Z, Yang Y-W. Tetraphenylethylene-Interweaving Conjugated Macrocycle Polymer Materials as Two-Photon Fluorescence Sensors for Metal Ions and Organic Molecules. *Adv. Mater.* **30**, 1800177 (2018).
37. Deng H, *et al.* A simple approach to prepare isoxazoline-based porous polymer for the highly effective adsorption of 2,4,6-trinitrotoluene (TNT): Catalyst-free click polymerization between an in situ generated nitrile oxide with polybutadiene. *Chem. Eng. J.* **393**, 124674 (2020).
38. Ho Y-S. Review of second-order models for adsorption systems. *J. Hazard. Mater.* **136**, 681-689 (2006).
39. Yang L, Chang G, Wang D. High and Selective Carbon Dioxide Capture in Nitrogen-Containing Aerogels via Synergistic Effects of Electrostatic In-Plane and Dispersive π–π-Stacking Interactions. *ACS Appl. Mater.Interfaces* **9**, 15213-15218 (2017).

Figures

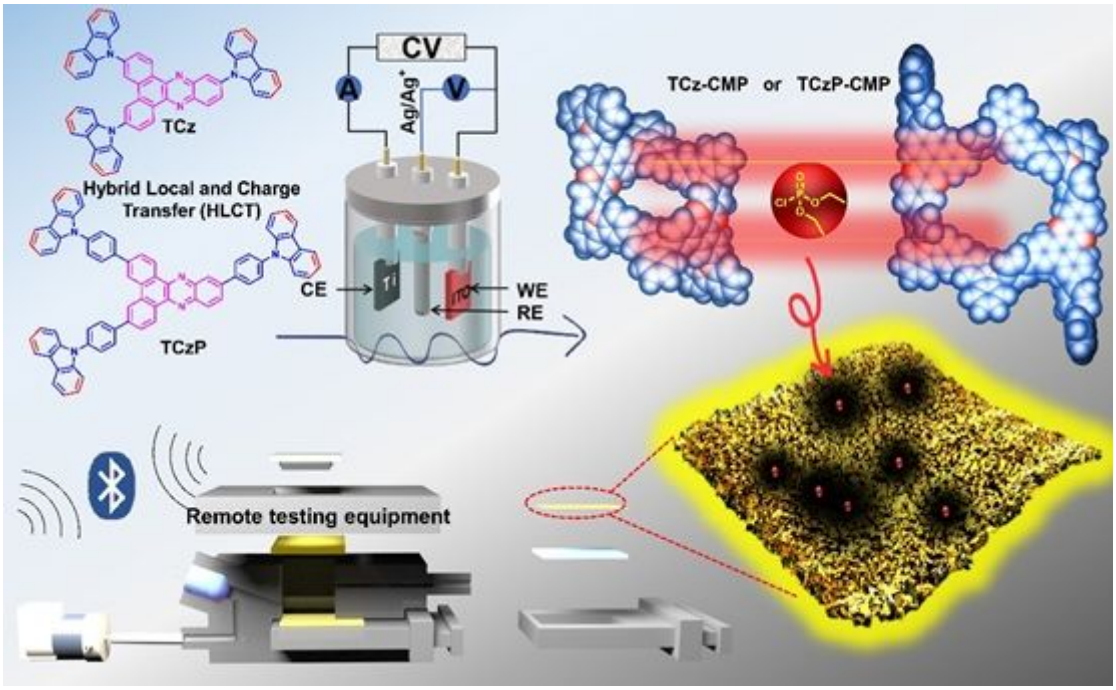

Figure 1

Scheme of sensor design. The chemical structures of TCzP and TCz with HLCT excited states, and their CMP films prepared by EP are used in lightweight, wireless and portable detection equipment.

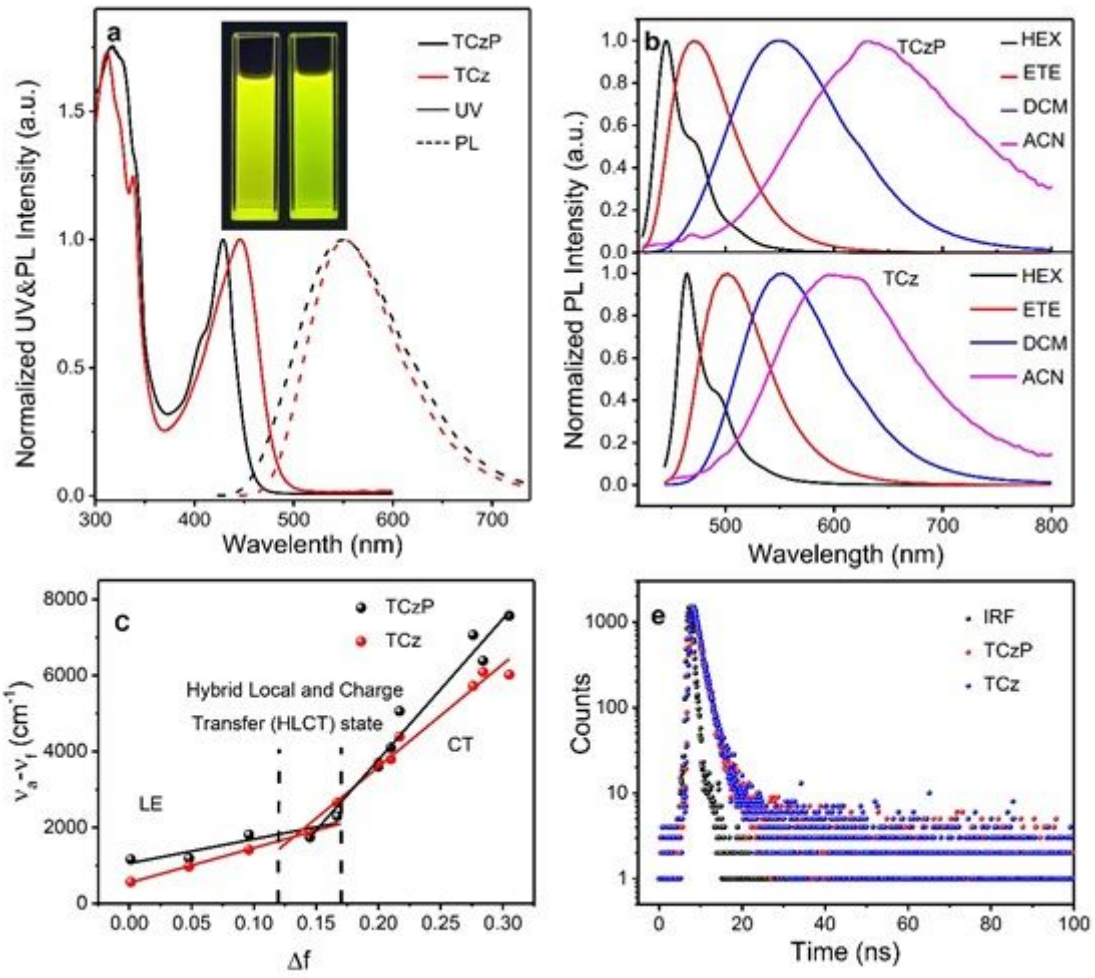

Figure 2

Optical properties of polymer precursors. a The UV-Vis and PL spectra of TCz and TCzP in DCM. Inset: the photo shows the fluorescence of TCzP (left) and TCz (right) in DCM solution excited by a wavelength of 365 nm. b The solvatochromic effects of TCz and TCzP in the increasing polarity solvent (HEX, ETE, DCM and ACN). c Solvatochromic Lippert-Mataga models of TCz and TCzP. d Transient PL spectra of TCz and TCzP in isopropyl ether.

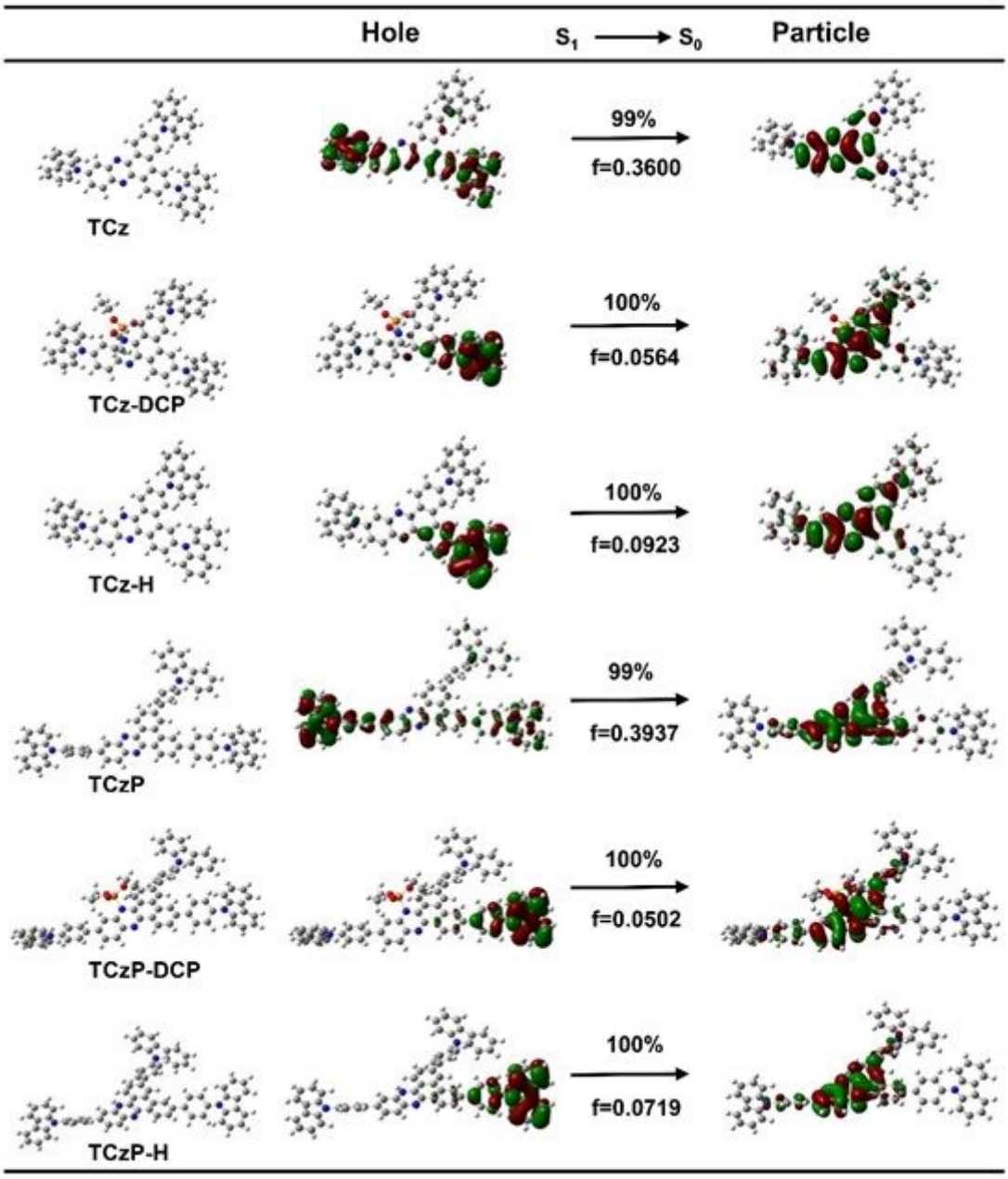

Figure 3

Calculated Excited State Properties. The NTO analysis of S1→S0 transition for TCz and TCzP before and after exposure to DCP.

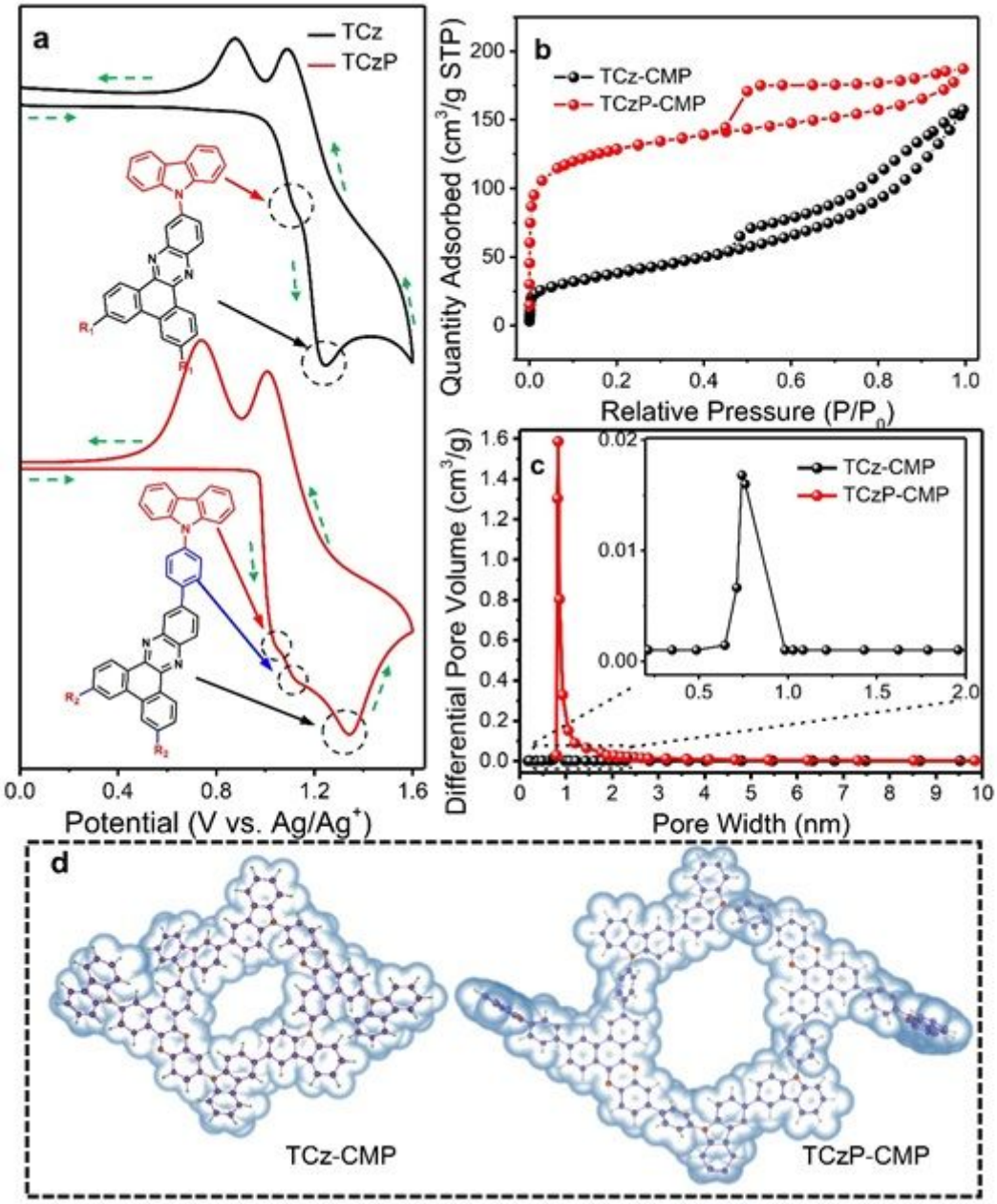

Figure 4

The preparation of CMP films and pore size analysis. a The single-cycle CV curve of TCz and TCzP with the scanning potential of 0-1.5 V. b Nitrogen adsorption/desorption curve of TCz-CMP and TCzP-CMP. c Pore size distribution curves of TCz-CMP and TCzP-CMP. d The optimal configuration of TCz (left) and TCzP (right) calculated by TD-DFT.

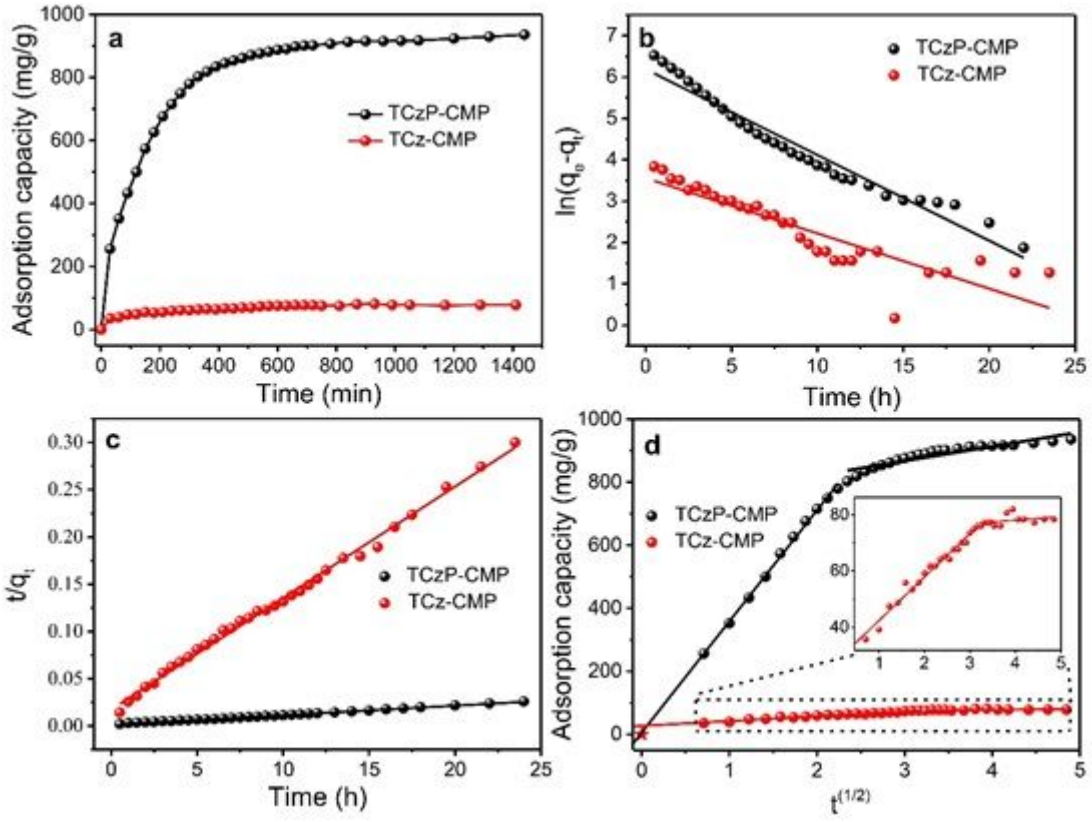

Figure 5

Adsorption performance of CMP to DCP vapors. a Adsorption capacity of the TCz-CMP and TCzP-CMP to DCP; b PFO model; c PSO model; d intraparticle diffusion model.

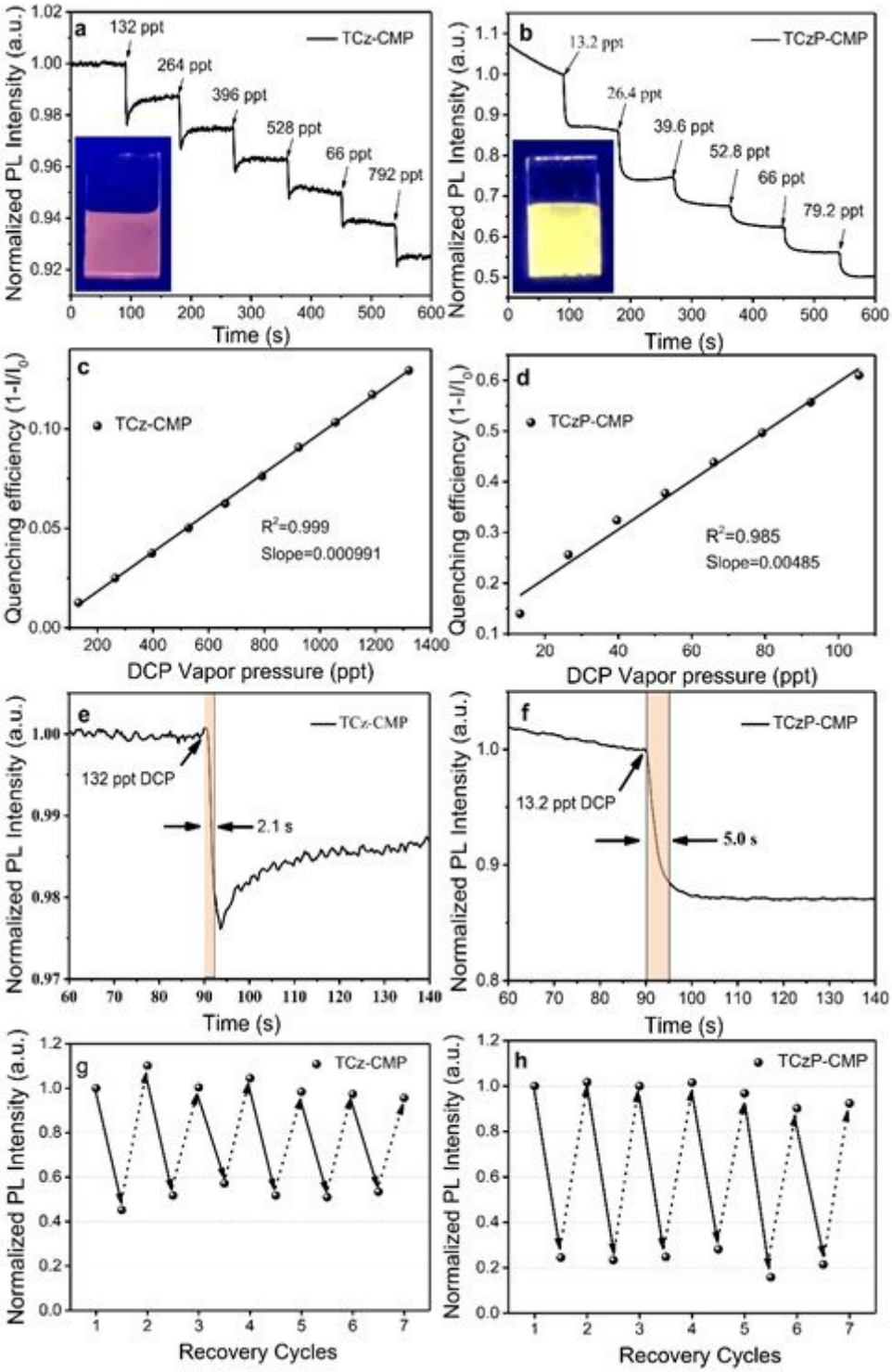

Figure 6

Sensing performance of CMP films. a-b Time-dependent fluorescence intensity of TCz-CMP and TCzP-CMP films changes after exposure to DCP vapors, inset is the photo of the CMP films under the excitation at 365 nm. c-d The quenching efficiency of TCz-CMP and TCzP-CMP films to DCP vapors. e-f Response time of TCz-CMP and TCzP-CMP films to DCP vapors. g-h The recovery test of TCz-CMP and TCzP-CMP films to DCP vapors (Solid arrow: the quenching process; Dash arrow: the recovery process).

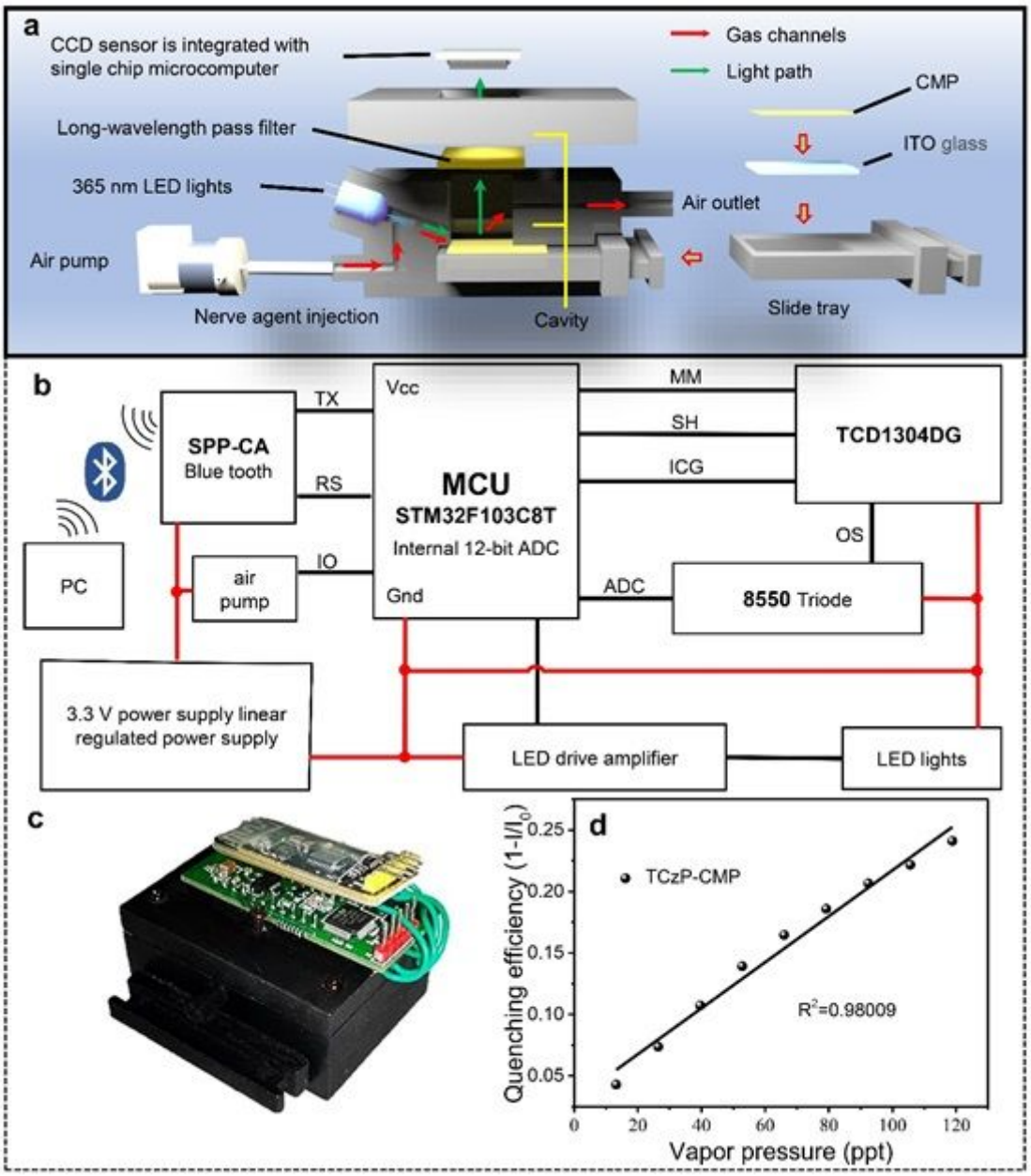

Figure 7

Device design and testing. a The internal structure diagram of the portable detection system. b Schematic diagram of the circuit of the detection system. c Photos of the portable detection system. d The quenching efficiency of the TCzP-CMP films mounted in the portable detection system to DCP vapors.

Supplementary Files

This is a list of supplementary files associated with this preprint. Click to download.

- SupportingInformation.docx